Inorganic Chemistry

pubs.acs.org/IC

Featured Article

Aerobic Partial Oxidation of Alkanes Using Photodriven Iron Catalysis

Nathan Coutard, Jonathan M. Goldberg, Henry U. Valle, Yuan Cao, Xiaofan Jia, Philip D. Jeffrey, T. Brent Gunnoe,* and John T. Groves*

Cite This: *Inorg. Chem.* 2022, 61, 759−766

Read Online

ACCESS | Metrics & More | Article Recommendations | Supporting Information

ABSTRACT: Photodriven oxidations of alkanes in trifluoroacetic acid using commercial and synthesized Fe(III) sources as catalyst precursors and dioxygen (O_2) as the terminal oxidant are reported. The reactions produce alkyl esters and occur at ambient temperature in the presence of air, and catalytic turnover is observed for the oxidation of methane in a pure O_2 atmosphere. Under optimized conditions, approximately 17% conversion of methane to methyl trifluoroacetate at more than 50% selectivity is observed. It is demonstrated that methyl trifluoroacetate is stable under catalytic conditions, and thus overoxidized products are not formed through secondary oxidation of methyl trifluoroacetate.

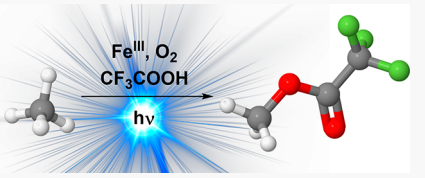

INTRODUCTION

There is great interest in the fundamental chemistry of hydrocarbon partial oxidation via C−H bond activation using dioxygen (O_2) as the terminal oxidant. However, despite extensive research, the selective partial oxidation of alkanes stands among the most challenging chemical reactions.[1] The high bond dissociation energy of alkane C−H bonds (typically >96 kcal/mol) combined with the often weaker C−H bonds of functionalized products frequently leads to cascading oxidation reactions and undesirable overoxidation, including the production of carbon dioxide (CO_2).[2] As a result, current industrial processes for the production of methanol from methane rely on an indirect route involving the conversion of methane to synthesis gas [i.e., syngas, carbon monoxide (CO)/dihydrogen], which is energy- and capital-intensive.[3] Hence, there is motivation for new processes for the direct partial oxidation of alkanes under ambient conditions.[4] While examples of thermal alkane partial oxidation using transition metals have been reported, many of them either have not been tested for light alkanes,[5] yield overoxidized products,[6] require complex catalysts and/or multistep and energy-intense extraction procedures,[6a,7] or make use of terminal oxidants not recycled by O_2, preventing industrial viability.[8]

The Catalytica process, which uses a Pt(II) catalyst in oleum, stands out because it provides high selectivity and the conversion of methane to methyl bisulfate, which can be hydrolyzed to form methanol.[9] Catalytic conversion of methane to methyl bisulfate has been demonstrated for other electrophilic catalysts [i.e., in addition to Pt(II)] in superacidic media.[10] However, drawbacks of such processes include the susceptibility of the electrophilic metal center to poisoning by even strong acids and the energy-intensive process required to separate methyl bisulfate from oleum.

Recently, there has been growing interest in photodriven C−H functionalization with some advancements on strategies for C−C coupling.[11] Photochemistry can allow the selective formation of high-energy intermediates that cannot be obtained thermally. However, there is little precedent regarding the photolytic conversion of light alkanes, and only a few publications report the oxidation of nonfunctionalized alkanes using photocatalysis. Turnovers (TOs) are attained for the conversion of light alkanes to *tert*-butoxycarbonyl-protected hydrazines using cerium chloride photocatalysts.[12] The selective conversion of methane to methanol using a TiO_2-supported Fe catalyst and hydrogen peroxide (H_2O_2) as a terminal oxidant was reported,[13] as well as aqueous photooxidation of methane to methanol with perrhenate salts.[14] Previously, our groups have reported oxyesterification of light alkanes in trifluoroacetic acid (HTFA), in both thermal and photolytic processes,[15a−d] and the group of Goldberg and Schelter have reported an aerobic photocatalytic process for alkane iodination.[15e]

RESULTS AND DISCUSSION

We screened a series of commercial, air-stable Fe(III) compounds for alkane photooxidation. For these initial screens, we used reactions that are stoichiometric in Fe(III). Iron 1,3,5-benzenetricarboxylate (Fe-BTC) and $[Et_4N]FeCl_4$ previously have been shown to functionalize C−H bonds of cyclohexane and toluene in organic solvents under photo-

Received: October 4, 2021
Published: December 28, 2021

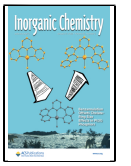

https://doi.org/10.1021/acs.inorgchem.1c03086
Inorg. Chem. 2022, 61, 759−766

chemical conditions in the presence of an external oxidant (air/O_2).[16] For our initial screening, Fe(III) compounds (0.25 mmol) were combined with HTFA and cyclohexane (1.25 mmol), and the mixture was irradiated with a 370 nm light-emitting diode (LED) for 24 h (Table 1). Of the Fe compounds we examined, commercial iron(III) trifluoromethanesulfonate [$Fe(OTf)_3$] performed the best, giving a quantitative yield of cyclohexyl trifluoroacetate (Cy-TFA), based on the amount of Fe(III), with no detectable overoxidation (e.g., cyclohexanone or difunctionalized products). The quantitative yield based on Fe(III) is the theoretical maximum for a two-electron reaction, assuming that two Fe(III) centers are required for the conversion of cyclohexane and HTFA to Cy-TFA [note: these initial screening reactions were stoichiometric in Fe(III)]. The quantum yield for this process was determined to be ~1% using standard iron oxalate actinometry, although this value is certainly an underestimate because of the turbidity of the reaction mixture (see the Supporting Information, SI). $Fe(acac)_3$ (acac = acetylacetonate), which contains three bidentate κ^2-O,O acac ligands, gave moderate functionalization with only 26% yield over the same time period. We hypothesize that the bidentate acac ligands are bound too strongly to allow full conversion to the proposed active Fe species that is responsible for C−H functionalization over the time allowed for the reaction (24 h, *vide infra*). LEDs can generate heat, resulting in the reactors reaching temperatures of 40−50 °C. In a control experiment performed in the dark for 24 h at 60 °C, no cyclohexane functionalization was detected, demonstrating the photochemical nature of the reaction.

With these promising results selectively activating a single C−H bond in cyclohexane, the scope of substrates was expanded to other alkanes. C−H functionalization was observed using $Fe(OTf)_3$ for methane, ethane, propane, cyclopentane, and *n*-pentane (Table 2). Yields against n_{Fe} are

Table 1. Screening of Fe(III) Compounds for Photochemical Cyclohexane Functionalization[a]

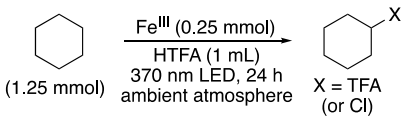

entry	Fe(III) source	yield $f(n_{Fe})$
1	none	ND
2	none (0.75 mmol of HOTf)	ND
3	Fe_2O_3	trace
4[b]	Fe_3O_4	<1%
5[c]	$Fe(acac)_3$	26%
6	$[Et_4N]FeCl_4$	100%[d,e]
7[c]	Fe-BTC	96%
8	$Fe(OTf)_3$	100%
9[f]	$Fe(OTf)_3$	18%

[a]Yields based on the amount of iron, abbreviated as $f(n_{Fe})$, are determined by GC−MS versus tetradecane as an internal standard and are the average of two experiments. [b]Both Fe_2O_3 and Fe_3O_4 are only partially soluble in TFA, affording inactive Fe_3-μ_3O upon dissolution (see below). For Fe_3O_4, 0.26 mmol was used. Yield based on the equivalents of Fe_3O_4 and does not account for reaction stoichiometry in footnote a. [c]Detected <5% Cy-1,2-TFA. [d]18% Cy-TFA; 82% Cy-Cl. [e]Trace cyclohexanone detected. [f]Blue LED (400−500 nm) used instead of 370 nm. ND = not detected.

Table 2. Screening Substrates for Photooxidation Using $Fe(OTf)_3$ in HTFA

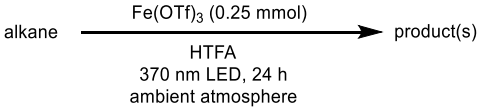

Entry	Alkane	Product(s)	Yield f(n$_{Fe}$)
1[a]	CH_4	CH_3TFA	60 ± 4%
2[a]	C_2H_6	TFA	36 ± 2%
		TFA-TFA	ND
3[a]	C_3H_8	TFA	140 ± 24%
		TFA	64 ± 14%
		TFA-TFA	ND
4[b]		TFA	50%
5[b]		TFA	52%
		TFA	30%
6[b]		TFA	100%
7[b]		TFA	56%
		TFA	34%

[a]Alkane (gaseous, 100 psig), HTFA (8 mL), and a 90 mL Fisher-Porter pressure reaction vessel. [b]Alkane (liquid, 1.25 mmol), HTFA (1 mL), and a 8 mL microwave vial with crimp cap. Yields averaged from three[a] or two[b] experiments, measured by NMR[a] or GC−MS[b]. ND = not detected. Typical NMR or GC−MS spectra for the characterization of products for each of the above reactions can be found in the SI for all substrates: methane (Figure S9), ethane (Figure S10), propane (Figure S11), and liquid alkanes (Figures S15−S18). The observation of CHF_3 and CHF_2TFA is discussed below.

60% for MeTFA and 36% for EtTFA, and the combined yield for propane oxidation products reached ~2 TOs. For all substrates, the TFA monoester was the major product. In the case of propane, preference for 2-propyl trifluoroacetate over 1-propyl trifluoroacetate in an approximate 2:1 ratio is consistent with a process involving net homolytic H-atom abstraction, selecting for the weaker internal C−H bond over the stronger terminal C−H bond.[15a−d] While the difference in yields between methane, ethane, and propane cannot be directly correlated to the strength of the C−H bonds, similar observations were reported for the photoamination of light alkanes by cerium salts, with the solubility of different alkanes impacting reaction yields.[12] The observation of CHF_3 and CHF_2TFA for some reactions is discussed below.

Combining each of the active Fe compounds in Table 1 with alkanes in HTFA results in heterogeneous mixtures. After removal of the solids by filtration, the soluble fractions gave the same absorbance feature in UV−vis spectra at ~340 nm (Figure S1). This common feature suggests *in situ* formation of the same soluble Fe species. In separate experiments, we monitored the formation of Cy-TFA over time using $Fe(OTf)_3$ and $Fe(TFA)_3$ as Fe(III) sources (Figure 1). Both reactions give near-quantitative formation of Cy-TFA after 24 h of photolysis. When using $Fe(OTf)_3$, an induction period, followed by the rapid formation of Cy-TFA, was observed, while the $Fe(TFA)_3$ plot appears to be approximately linear, suggesting that Fe(III) salts initially undergo a reaction with the HTFA solvent to form an Fe(III) complex that mediates

https://doi.org/10.1021/acs.inorgchem.1c03086
Inorg. Chem. 2022, 61, 759−766

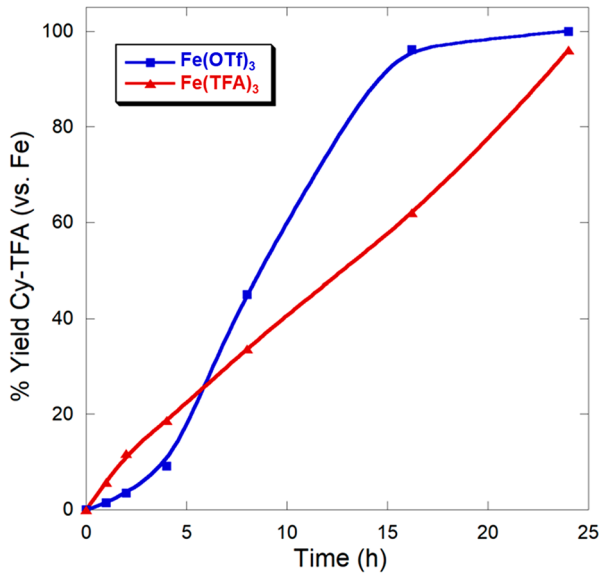

Figure 1. Cy-TFA production by the photolysis of Fe(III)/HTFA mixtures with a 370 nm LED. Each point on the plot resulted from a separate reaction. The lines are added to guide the eye. Conditions: 0.25 mmol of Fe(III), 1.25 mmol of cyclohexane, 1 mL of HTFA, and a 8 mL microwave vial with crimp cap. The photoreduction of Fe(III) to Fe(II) followed a similar time course (Figure S19).

alkane oxidation. The relatively poor activity of $Fe(acac)_3$ compared to complexes (see above) with more labile ligands is consistent with the strong coordination of acac.

In excess HTFA, the Fe(III) salts react to form $Fe^{III}_x(TFA)_y$ clusters.[17] A previous report showed that refluxing anhydrous $Fe^{III}Cl_3$ in HTFA leads to the formation of a hygroscopic white solid described as "$Fe(TFA)_3$".[18] Upon exposure to moisture, this white solid changes color to form a red material, the structure of which was later reported.[19] We were able to crystallize a similar structure (CCDC 2096583; Figure S2 and Tables S1–S9) as $[Fe^{III}_3(\mu_3\text{-O})(H_2O)_2(\mu\text{-TFA})_6(TFA)]$-(HTFA), termed "$Fe_3$-$\mu_3$O" herein. The structure shows that three Fe(III) ions are arranged around a central μ_3-bridging oxo coplane with three Fe(III) atoms. Two of the Fe atoms have water (H_2O) molecules coordinated trans to the μ_3-oxo bridge and have short Fe–oxo bond distances [1.912(2) Å]. The third iron–oxo bond distance is longer (1.955 Å), reflecting the *trans*-trifluoroacetate ion on that Fe. Although the structure that we determined for $[Fe^{III}_3(\mu_3\text{-O})(H_2O)_2(\mu\text{-TFA})_6(TFA)](HTFA)$ is similar to the previously reported structure,[19] one of the protons in the aqua ligands in the structure is resolved and involved in a hydrogen bond with a disorganized solvent molecule rather than with the F atom of a clearly defined TFA ligand. Fe_3-μ_3O was further characterized using Mössbauer and electron paramagnetic resonance (EPR) spectroscopy (Figures S13 and S14), which show characteristics typical of high-spin ferric iron.

We studied the effect of O_2 and H_2O on methane oxidation using freshly prepared anhydrous $Fe(TFA)_3$ handled in an anaerobic environment (Table 3). While O_2 was required to oxidize methane to MeTFA using $Fe(TFA)_3$, the presence of H_2O was detrimental to activity. For example, adding 2 equiv [relative to the amount of $Fe(TFA)_3$] of H_2O under 1 atm of dry O_2 reduced MeTFA yield from ~200% (i.e., two catalytic TOs) to 34% (entries 2 and 3, Table 3). Adding 22 equiv of H_2O rendered $Fe(TFA)_3$ entirely inactive (entry 6, Table 3).

Table 3. Screen of Conditions for Methane Oxidation with $Fe(TFA)_3$[a]

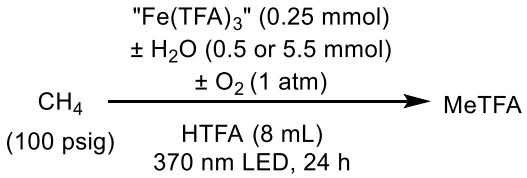

entry	O_2	H_2O	yield $f(n_{Fe})$
1	reaction carried in air	33 ± 2%	
2[b]	+	+	34 ± 5%
3[c]	+	–	196 ± 13%
4[b]	–	+	trace
5[c]	–	–	ND
6[d]	+	++	ND

[a]Standard reaction conditions: 0.25 mmol of $Fe(TFA)_3$, 100 psig of CH_4, 8 mL of HTFA, 370 nm LED, and a 90 mL Fisher-Porter pressure reaction vessel. Yields were determined by ^1H NMR spectroscopy with CH_3NO_2 as an internal standard. HTFA and H_2O were degassed with N_2. Yields are averaged from triplicate experiments. ND = not detected. Trace = yield <1%. [b]A total of 0.5 mmol of H_2O was added. [c]To remove all H_2O, reaction carried in 8 mL of HTFA/TFAA in a 4:1 volume ratio. TFAA is trifluoroacetic anhydride. [d]A total 5.5 mmol of H_2O was added.

These results indicate that the active species for alkane oxidation is not the Fe_3-μ_3O complex. Thus, we propose that $Fe(TFA)_3$ is the active species for hydrocarbon oxidation but can react with H_2O to form the inactive Fe_3-μ_3O complex. Thus, under aerobic conditions, because the hydrocarbon is oxidized and H_2O is formed, inhibition of catalysis is anticipated (Scheme 1).

Scheme 1. Oxidation of Methane by O_2 in HTFA, Followed by Formation of the Inactive $[Fe^{III}_3(\mu_3\text{-O})(H_2O)_2(\mu\text{-TFA})_6(TFA)](HTFA)$, through the Reaction of $Fe(TFA)_3$ with H_2O

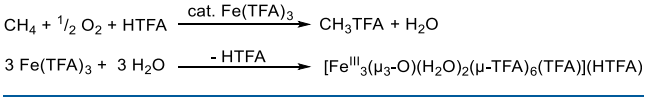

The hypothesis that an inactive species is formed in the presence of H_2O is supported by UV–vis characterization of $Fe(TFA)_3$ in different solvent mixtures (Figure 2). $Fe(TFA)_3$ is insoluble in rigorously dry HTFA and gives no discernible features in the UV–vis spectrum. Upon the addition of H_2O, red Fe_3-μ_3O is formed, characterized by an absorption at 338 nm. $Fe(TFA)_3$ is soluble in dry acetonitrile with characteristic absorption features at 313 and 359 nm. The addition of H_2O makes these features disappear with the concomitant appearance of the characteristic Fe_3-μ_3O feature at 338 nm.

Because H_2O is an expected byproduct of methane oxidation using O_2, we added trifluoroacetic anhydride (TFAA) to a methane photooxidation reaction to trap byproduced H_2O before it could poison the catalyst. Under these conditions, the amount of MeTFA formed is a direct function of n_{O_2} (n_{MeTFA} = 0.14 ± 0.01 n_{O_2}), supporting the role of O_2 as the terminal oxidant (Figure S3). With a large excess of O_2, up to 24 TOs of MeTFA and ~17% conversion of methane could be obtained (Scheme 2). High methane conversion could not be reached at high TO, which we attribute to the degradation of $Fe(TFA)_3$

https://doi.org/10.1021/acs.inorgchem.1c03086
Inorg. Chem. 2022, 61, 759–766

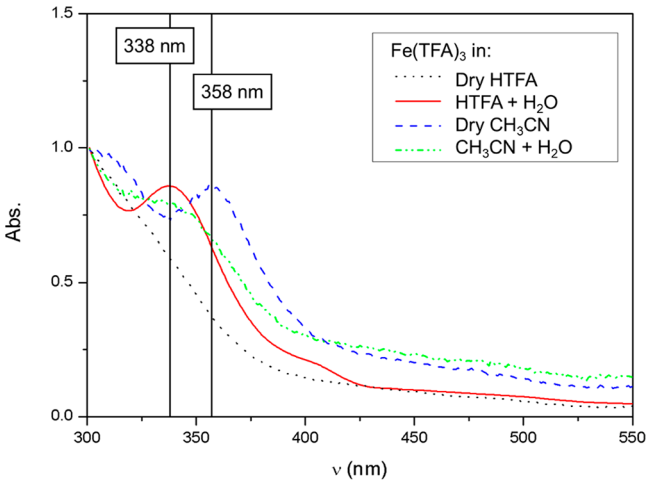

Figure 2. UV−vis spectra of $Fe(TFA)_3$ in dry HTFA, HTFA/H_2O mixture (20:1 ratio by volume), dry CH_3CN, and a CH_3CN/H_2O mixture (20:1 ratio by volume).

Scheme 2. Photooxidation of Methane by $Fe(TFA)_3$ in Excess O_2[a]

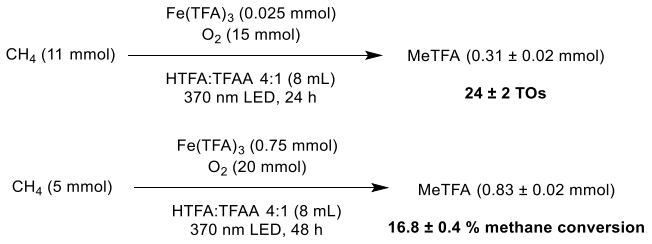

[a]In the absence of $Fe(TFA)_3$, MeTFA is not observed. Where the TOs are measured, we assume that 2 equiv of Fe(III) is required for each conversion of methane and HTFA to MeTFA. Standard deviations based on a minimum of three independent experiments.

because it likely oxidizes the solvent at lower methane concentrations.

A key challenge for the selective partial oxidation of light alkanes is overoxidation, which is often a result of the intrinsically high reactivity of functionalized alkyl products compared with starting alkanes. To determine the potential efficacy of Fe-catalyzed photodriven hydrocarbon partial oxidation, we compared the rate of MeTFA formation from methane to the rate of MeTFA consumption under reaction conditions. The degradation rate of MeTFA under reaction conditions was assessed and shown to be much slower than the rate of its formation, with >90% MeTFA remaining after 24 h (Figure 3). Regardless of the mechanism for the formation of MeTFA, the monooxidized product is stable under reaction conditions, indicating a protective effect of the ester moiety.[15] Under the conditions in Figure 3, the different solubilities of methane and MeTFA play a role. While methane oxidation proceeds under ideal conditions (before substrate depletion or catalyst decomposition), the rate of MeTFA formation is ∼16 times faster than the rate of MeTFA degradation. Hence, any significant CO_2 production does not likely originate from overoxidation of MeTFA, demonstrating the viability of high selectivity at high conversion of methane.

A pressurized J. Young NMR tube was used to observe gaseous, proton-containing byproducts. Upon photolysis of $Fe(TFA)_3$ in HTFA with 50 psig of methane, we detected

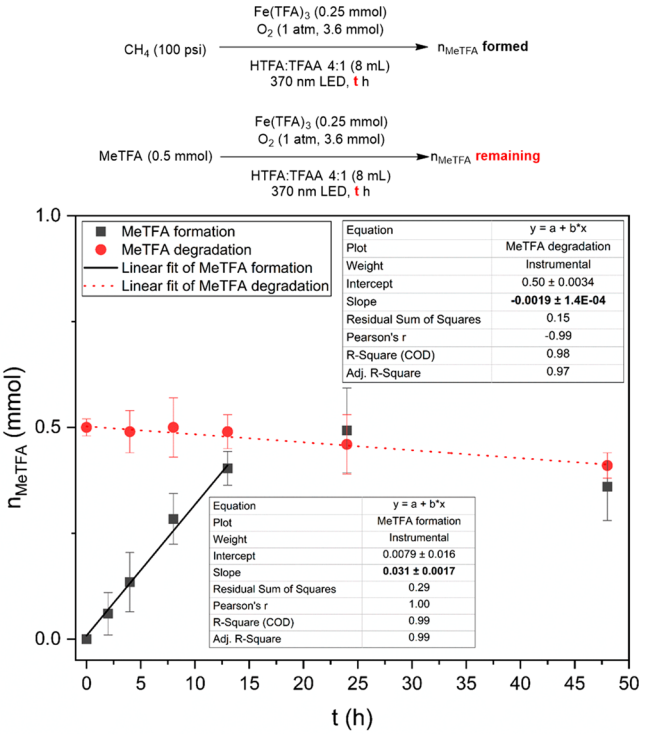

Figure 3. Rate of formation (black squares) and degradation (red dots) of MeTFA under photolytic conditions (see the equations above the plot for conditions). The data for MeTFA degradation are fitted linearly between 0 and 48 h, and the data for MeTFA formation are fitted between 0 and 12 h.

difluoromethyl trifluoroacetate ($CHF_2CO_2CF_3$; δ = 6.91 ppm, triplet, $^2J_{HF}$ = 70 Hz) and trace trifluoromethane (CHF_3; δ = 6.18 ppm, quartet, $^2J_{HF}$ = 80 Hz),[20] both of which are known HTFA degradation products (Figure 4).[21] When the methane was replaced with Ar, both $CHF_2CO_2CF_3$ and CHF_3 were observed, but the formation of MeTFA was not detected (Figure 4). Furthermore, upon replacement of HTFA with deuterated trifluoroacetic acid (DTFA), only trace $CHF_2CO_2CF_3$ and CHF_3 were observed under either an Ar or CH_4 atmosphere. Under these conditions, the formation of small amounts of $CHF_2CO_2CF_3$ and CHF_3 likely arise from trace protio-HTFA remaining in DTFA. These observations point to HTFA degradation, and not that of methane, as the origin of these byproducts. This was also observed for the oxidation of substrates with weaker C−H bonds than that of methane, such as propane (Figure S4) and cyclohexane (Figure S12) in DTFA/TFAA. However, CHF_3 formation during the oxidation of cyclohexane was observed even in DTFA/TFAA, pointing to the more reactive nature of the cyclohexane C−H bond compared to that of lighter alkanes, and the consequent ability of a CF_3 radical to abstract this H atom.

Gaseous byproducts were quantified at 17% conversion of methane to MeTFA through headspace analysis using a gas chromatography with a thermal conductivity detector (GC-TCD). Trace CO (<0.1% yield) was observed; however, no ethane or ethylene was detected. Evidence of CO_2 formation was obtained in the headspace of reactions with either CH_4 or Ar (without CH_4), leading to the conclusion that part of CO_2 was a product of solvent oxidation (HTFA) rather than methane overoxidation (Figures S5 and S7). Labeled $^{13}CH_4$ allowed us to assess the quantity of CO_2 arising from methane

https://doi.org/10.1021/acs.inorgchem.1c03086
Inorg. Chem. 2022, 61, 759−766

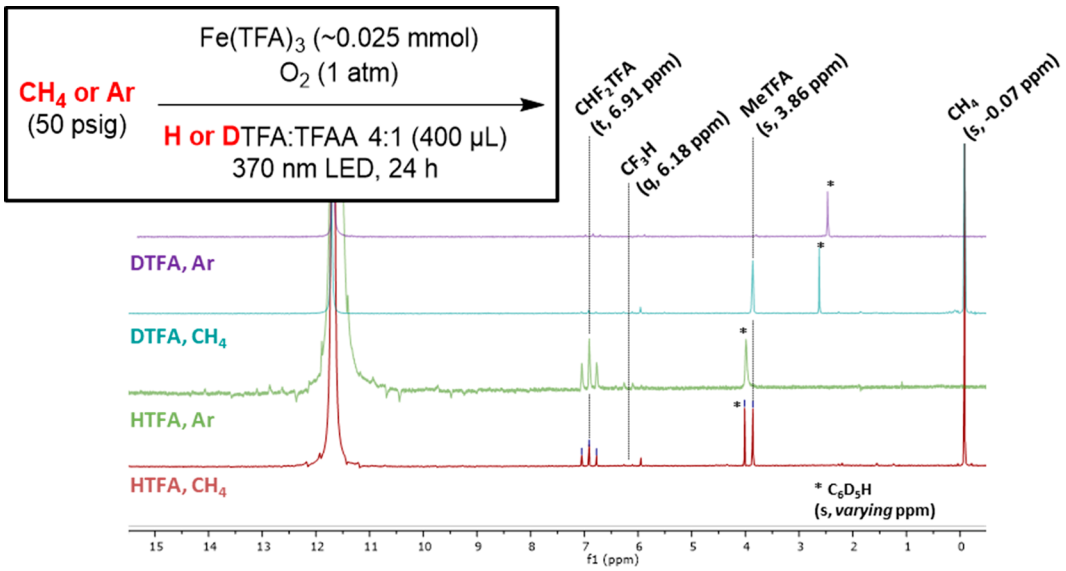

Figure 4. 500 MHz ^{1}H NMR spectra resulting from the illumination of $Fe(TFA)_3$ with a 370 nm LED light under different conditions of solvent and headspace. A C_6D_6 capillary was used as a locking solvent for the NMR. The signal of residual C_6D_5H for the lock solvent is observed at unpredictable shift values due to paramagnetic shifts of the reaction media, which does not shift the C_6D_5H signal in the sealed capillary. Use of a coaxial NMR tube insert did not fix this variability. The addition of tetramethylsilane (TMS) to the capillary tube showed consistent separation of the C_6D_5H and TMS peaks, with both signals shifted from peaks arising from the reaction mixture (Figure S12). Spectra are hence referenced using either CH_4 (s, −0.07 ppm) or CHF_2TFA (t, 6.91 ppm).

overoxidation through gas chromatography−mass spectrometry (GC−MS; Figure S8). At 14% conversion of $^{13}CH_4$ to ^{13}MeTFA, the selectivity for ^{13}MeTFA was 56%, with the remainder being 44% $^{13}CO_2$ and trace (<0.1%) CO. Because of the stability of MeTFA under reaction conditions (Figure 3), we believe that CO_2 does not come from the oxidation of MeTFA but is rather formed by a different, and unknown, reaction pathway, possibly degradation of a reactive intermediate species. This is encouraging when considering the possible use of differently coordinated Fe(III) or other transition-metal photocatalysts to improve selectivity.

SUMMARY AND CONCLUSIONS

We report here new reactivity for several commercial Fe(III) salts for the photooxidation of a variety of linear and cyclic alkanes, C1−C6. From our initial observations, we concluded that a range of Fe(III) sources soluble in HTFA converged toward a common pathway, leading us to investigate a likely formed complex, $Fe(TFA)_3$, as the active species. We found this complex active for the oxidation of methane, and we characterized a poisoned state of the catalyst that arose from the reaction of the active species with H_2O. Because H_2O is an expected byproduct of alkane oxidation, we developed conditions that remove H_2O as the reaction proceeded and observed catalytic TO for the oxidation of methane to MeTFA. Notably, O_2 was determined to be the terminal oxidant, and 17% conversion of methane to the monoester product was attained at more than 50% selectivity.

EXPERIMENTAL METHODS

Caution! *Many of the reagents and conditions described herein are hazardous. Trifluoroacetic acid (HTFA) is highly corrosive and should be handled inside a fume hood with long nitrile gloves covering up to the elbow. LED lamps produce high-intensity UV light and direct eye or skin contact should be avoided. Appropriate safety procedures should be consulted prior to handling concentrated acids, strong oxidants, and mixtures of hydrocarbon substrates and* O_2.

General Considerations. All reactions were carried out under an ambient atmosphere unless otherwise stated. HTFA, cyclohexane, chlorocyclohexane, anhydrous $FeCl_3$, Fe_2O_3, Fe_3O_4, $Fe(acac)_3$, $[Et_4N]FeCl_4$, iron 1,3,5-benzenetricarboxylate (Fe-BTC), $Fe(OTf)_3$, tetradecane, and *tert*-butanol were purchased from commercial sources and used as received. Polytetrafluoroethylene (PTFE) filters (0.45 μm) were purchased from Fisher. Dioxygen (O_2; 99.6% purity) was purchased from Sigma-Aldrich and used as received. Authentic cyclohexyl trifluoroacetate (Cy-TFA) and 1,2-bis(trifluoroacetoxy)-cyclohexane were prepared according to a published procedure.[22] $Fe(TFA)_3$ and $Fe(TFA)_3{\cdot}xH_2O$ were prepared according to published procedures with a slight modification to include Apiezon PFPE 501 as the grease used to connect the round-bottom flask to the reflux condenser.[18] Microwave vials were purchased from Biotage and used as received. Teflon stoppered flasks (10 mL) were purchased from Chemglass and used as received. The 370 nm LED is a Kessil PR160-370 40 W LED and was used as received. The blue LED (400−500 nm) is a Kessil H150-blue 30 W high-luminous DEX 2100 LED and was used as received. GC−MS analysis was performed using an Agilent Technologies 7890A gas chromatograph equipped with a fused-silica column (crossbond 35% dipheny polysiloxane−65% dimethylpolysiloxane; 30 m × 0.32 mm; 0.5 μm thickness) and an electron impact mass analyzer. GC-TCD analysis was conducted in a Shimadzu GC-2014 gas chromatograph. UV−vis spectral measurements were recorded on an Agilent 8453 diode-array spectrophotometer at room temperature, with a 1-cm-path-length quartz cuvette. Zero-field ^{57}Fe Mössbauer spectra were recorded on a SEE Co. Mössbauer spectrometer (MS4) at 80 K in constant-acceleration mode. ^{57}Co/Rh was used as the radiation source. *WMOSS* software was used for quantitative evaluation of the spectral parameters (least-squares fitting to Lorentzian peaks). The temperature of the sample was controlled by a Janis Research Co. CCS-850 He/N2 cryostat within an accuracy of 0.3 K. Isomer shifts were determined relative to α-Fe at 298 K. EPR was recorded on a Bruker EPR EMX Plus spectrometer. NMR spectra were recorded on a Varian Inova 500 MHz spectrometer.

Photochemical Functionalization of Gaseous Light Alkanes by Fe(III) Compounds. A 90 mL glass Fisher-Porter reactor was charged with a stir bar, 0.25 mmol of an Fe(III) source, and HTFA (8 mL, 104.5 mmol). The reactor was then sealed and pressurized with

https://doi.org/10.1021/acs.inorgchem.1c03086
Inorg. Chem. 2022, 61, 759−766

alkane (methane, ethane, or propane) at 100 psig. The reactors were placed on a stir plate and irradiated with either a mercury lamp (Hanovia medium-pressure UV lamp, 450 W, Ace Glass) or two 370 nm LED lamps (Kessil PR-370). Following the reaction, the lamp(s) was (were) turned off, and the reactor was vented in a Tedlar sampling bag to keep for headspace analysis. For analysis of the liquid phase, an internal standard, either CH_3NO_2 or HOAc, was added to the reaction mixture in a known concentration to allow for the quantification of products. An aliquot was removed for centrifugation, and the supernatant was used for ^{1}H NMR analysis, following a previously published procedure from our laboratory.[15a,b] Unless otherwise mentioned, reactions were carried out in air. When air was excluded, the reactors were charged using a N_2 glovebox and a Schlenk line using N_2-degassed HTFA. When needed, dry O_2 was added by bubbling the vessel for 10 min. When needed, N_2-degassed H_2O was added through cannula transfer from a N_2-purged Schlenk flask. Representative ^{1}H NMR spectra resulting from the oxidation of methane, ethane, and propane are shown in Figures S9–S11, respectively.

Photochemical Functionalization of Liquid Alkanes by Fe(III) Compounds. Under an ambient atmosphere, an 8 mL microwave vial was charged with an Fe(III) source (0.25 mmol) and a stir bar. HTFA (1 mL) and liquid alkane (1.25 mmol) were added to the vial. The vial was sealed with a crimp cap containing a septum. The vial was placed ∼5 cm in front of a 370 nm LED (unless otherwise stated) and allowed to stir for 24 h. The reaction mixture was removed from the vial and filtered through a PTFE filter into a vial containing tetradecane (0.13 mmol). The reaction vial was rinsed with dichloromethane (5 mL) and filtered. The solutions were combined and washed two times with 10 mL of H_2O. The organic layer was eluted through a small silica plug to remove any trace Fe and then dried over $MgSO_4$. An aliquot was taken from the dichloromethane solution and analyzed by GC–MS to quantify Cy-TFA. Representative GC–MS data resulting from the oxidation of cyclohexane, cyclopentane, *n*-pentane, and *n*-hexane are shown in Figures S15–S18, respectively.

High Conversion and High TO Oxidation of Methane. To demonstrate possible catalytic TO, the amount of $Fe(TFA)_3$ was lowered to 0.025 mmol and a 4:1 mixture of HTFA/TFAA (8 mL) was used as the solvent. Then, 20 mmol of O_2 and 50 psig of methane were added, and the reaction was performed for 24 h. To reach higher conversion, the amount of $Fe(TFA)_3$ was increased to 0.75 mmol and the solvent was a 4:1 mixture of HTFA/TFAA (8 mL). Then, 15 mmol of O_2 and 50 psig of methane were added, and the reaction time was extended to 48 h.

Photochemical Functionalization of Alkanes in J. Young NMR Tubes. A J. Young NMR tube was charged with a capillary tube containing C_6D_6, 10 mg of $Fe(TFA)_3$, and a 4:1 mixture of H- or D-TFA/TFAA (400 μL). The tube was then purged with pure O_2, sealed and pressurized with 50 psig of either Ar, CH_4, or C_3H_8 or 1.25 mmol of cyclohexane. The tubes were irradiated with two 370 nm LED lamps (Kessil PR-370). Following the reaction, the lamp was turned off and NMR spectra were collected without opening the tubes to preserve the headspace pressure of the side products.

Preparation of UV–Vis Samples. An Fe(III) salt (0.25 mmol Fe) was combined with HTFA (1 mL) and cyclohexane (135 μL, 1.25 mmol), unless otherwise stated, to give a yellow/red mixture. The mixture was filtered through a PTFE filter and diluted to an optical density (OD) of <2. For samples in acetonitrile (MeCN), a corresponding Fe(III) salt was combined with MeCN (1 mL), filtered through a PTFE filter, and diluted to an OD of <2.

Headspace Analysis. After a reaction reached completion, the headspace of the reactors was depressurized in a Tedlar sampling bag, which was kept at −36 °C in a freezer until analysis of the sample. Analysis was conducted in a Shimadzu GC-2014 chromatograph equipped with a TCD by flushing a 500 μL injection loop with 1 mL of the gas headspace. The sample was first passed through a 1.0 m Hayesep T 80/100 column to trap solvent residue and moisture and then through a 1.5 m Hayesep Q 80/100 and 2.0 m MS5A 60/80 molecular sieve column using a custom dual-valve setup. The detector temperature was 200 °C, the current was 100 mA, and the column temperature was 75 °C. The injector temperature was 68 °C. A typical GC-TCD trace for the oxidation of methane with $Fe(TFA)_3$ is shown in Figure S7. The resulting integration yielded an amount of CO_2 as a volumetric fraction of total headspace, using independently measured calibration curves established from standards prepared with known volumetric fractions of CO_2 in CH_4 (Figure S6). A consistent detector response was seen when using CO_2/CH_4, CO_2/N_2, or CO_2/O_2 mixtures, with a given percent volume of CO_2 yielding statistically identical peak integration. These volumetric fractions were then converted to an amount of substance using the total headspace volume, measured by submitting the sampling bag to Archimedes' principle. To assess the isotopic ratio of $^{12}CO_2$ to $^{13}CO_2$, a portion (1 μL) of the headspace was injected in a GC–MS (Shimadzu GCMS-QP2010 Plus system with a Restek RT-Qbond 30 m × 8 mm fused-silica PLOT column with 8 μm thickness using electron impact ionization). GC–MS parameters: starting temperature, 40 °C; time at starting temp, 3 min; ramp, 20 °C/min up to 200 °C; flow rate (carrier), 3.01 mL/min (He); split ratio, 10:1; inlet temperature, 200 °C; detector ion source temperature, 200 °C; interface temperature, 230 °C. The CO_2 peak eluted at 2.97 min.

Sample Preparation for Low-Temperature EPR Analysis. EPR spectra were recorded on a Bruker EMX Plus spectrometer. Crystalline powders of $[Fe^{III}_3(\mu_3\text{-}O)(H_2O)_2(\mu\text{-}TFA)_6(TFA)]$-(HTFA) were prepared as a mixture with CH_3CN or HTFA in quartz tubes (Wilmad-LabGlass, quartz (CFQ) EPR tubes; 4 mm OD). The temperature-dependent measurements were conducted at 10 K using a continuous-flow cryostat (Oxford ESR900) with liquid He.

Sample Preparation for Zero-Field ^{57}Fe Mössbauer Analysis. Solid samples were sealed inside a nylon washer (0.5 in. inner diameter; 0.06 in. thickness) using two pieces of Kapton tape ($^3/_4$ in. diameter). The washer was affixed to a Cu sample mount. The mount was inserted into a Janis Research Co. He/N_2 cryostat at 80 K under a counterflow of He. The cryostat chamber was evacuated and refilled after 5 min with 1 atm of ultrahigh-purity-grade He. Data collection began after the sample temperature equilibrated at 80 K.

■ ASSOCIATED CONTENT

Supporting Information

The Supporting Information is available free of charge at https://pubs.acs.org/doi/10.1021/acs.inorgchem.1c03086.

Examples of NMR and UV–vis spectra, details of the single-crystal X-ray structure study, various plots of hydrocarbon conversions, details of CO_2 quantification, EPR spectra, and GC data (PDF)

Accession Codes

CCDC 2096583 contains the supplementary crystallographic data for this paper. These data can be obtained free of charge via www.ccdc.cam.ac.uk/data_request/cif, or by emailing data_request@ccdc.cam.ac.uk, or by contacting The Cambridge Crystallographic Data Centre, 12 Union Road, Cambridge CB2 1EZ, UK; fax: +44 1223 336033.

■ AUTHOR INFORMATION

Corresponding Authors

T. Brent Gunnoe − *Department of Chemistry, University of Virginia, Charlottesville, Virginia 22904, United States;* orcid.org/0000-0001-5714-3887; Email: tbg7h@virginia.edu

John T. Groves − *Department of Chemistry, Princeton University, Princeton, New Jersey 08544, United States;* orcid.org/0000-0002-9944-5899; Email: jtgroves@princeton.edu

https://doi.org/10.1021/acs.inorgchem.1c03086
Inorg. Chem. 2022, 61, 759–766

Authors

Nathan Coutard − *Department of Chemistry, University of Virginia, Charlottesville, Virginia 22904, United States*

Jonathan M. Goldberg − *Department of Chemistry, Princeton University, Princeton, New Jersey 08544, United States;* orcid.org/0000-0003-0495-6985

Henry U. Valle − *Department of Chemistry, Princeton University, Princeton, New Jersey 08544, United States;* orcid.org/0000-0001-7540-4083

Yuan Cao − *Department of Chemistry, Princeton University, Princeton, New Jersey 08544, United States*

Xiaofan Jia − *Department of Chemistry, University of Virginia, Charlottesville, Virginia 22904, United States;* orcid.org/0000-0003-0425-5089

Philip D. Jeffrey − *Department of Molecular Biology, Princeton University, Princeton, New Jersey 08544, United States*

Complete contact information is available at: https://pubs.acs.org/10.1021/acs.inorgchem.1c03086

Notes

The authors declare no competing financial interest.

■ ACKNOWLEDGMENTS

The authors thank Dr. Jonathan Darmon at Princeton University for help with the Mössbauer spectroscopy. This research was sponsored by the U.S. Department of Energy, Office of Energy Efficiency and Renewable Energy, Advanced Manufacturing Office, under Contract DE-AC05-00OR22725 with UT-Battelle, LLC.

■ REFERENCES

(1) (a) Stahl, S. S.; Labinger, J. A.; Bercaw, J. E. Homogeneous Oxidation of Alkanes by Electrophilic Late Transition Metals. *Angew. Chem., Int. Ed.* **1998**, *37* (16), 2180−2192. (b) Han, B.; Yang, Y.; Xu, Y.; Etim, U. J.; Qiao, K.; Xu, B.; Yan, Z. A review of the direct oxidation of methane to methanol. *Chinese Journal of Catalysis* **2016**, *37* (8), 1206−1215. (c) Horn, R.; Schlögl, R. Methane Activation by Heterogeneous Catalysis. *Catal. Lett.* **2015**, *145* (1), 23−39. (d) Webb, J. R.; Bolaño, T.; Gunnoe, T. B. Catalytic Oxy-Functionalization of Methane and Other Hydrocarbons: Fundamental Advancements and New Strategies. *ChemSusChem* **2011**, *4* (1), 37−49.

(2) (a) Tang, P.; Zhu, Q.; Wu, Z.; Ma, D. Methane activation: the past and future. *Energy Environ. Sci.* **2014**, *7* (8), 2580−2591. (b) Ravi, M.; Ranocchiari, M.; van Bokhoven, J. A. The Direct Catalytic Oxidation of Methane to Methanol—A Critical Assessment. *Angew. Chem., Int. Ed.* **2017**, *56* (52), 16464−16483.

(3) (a) Gunsalus, N. J.; Koppaka, A.; Park, S. H.; Bischof, S. M.; Hashiguchi, B. G.; Periana, R. A. Homogeneous Functionalization of Methane. *Chem. Rev.* **2017**, *117* (13), 8521−8573. (b) Zakaria, Z.; Kamarudin, S. K. Direct conversion technologies of methane to methanol: An overview. *Renewable Sustainable Energy Rev.* **2016**, *65*, 250−261. (c) Schwach, P.; Pan, X.; Bao, X. Direct Conversion of Methane to Value-Added Chemicals over Heterogeneous Catalysts: Challenges and Prospects. *Chem. Rev.* **2017**, *117* (13), 8497−8520.

(4) Meng, X.; Cui, X.; Rajan, N. P.; Yu, L.; Deng, D.; Bao, X. Direct Methane Conversion under Mild Condition by Thermo-, Electro-, or Photocatalysis. *Chem.* **2019**, *5* (9), 2296−2325.

(5) (a) Nagarjun, N.; Dhakshinamoorthy, A. Liquid phase aerobic oxidation of cyclic and linear hydrocarbons using iron metal organic frameworks as solid heterogeneous catalyst. *Molecular Catalysis* **2019**, *463*, 54−60. (b) Company, A.; Gómez, L.; Güell, M.; Ribas, X.; Luis, J. M.; Que, L.; Costas, M. Alkane Hydroxylation by a Nonheme Iron Catalyst that Challenges the Heme Paradigm for Oxygenase Action. *J. Am. Chem. Soc.* **2007**, *129* (51), 15766−15767.

(6) (a) Yu, X.; De Waele, V.; Löfberg, A.; Ordomsky, V.; Khodakov, A. Y. Selective photocatalytic conversion of methane into carbon monoxide over zinc-heteropolyacid-titania nanocomposites. *Nat. Commun.* **2019**, *10* (1), 700. (b) Almquist, C. B.; Biswas, P. The photo-oxidation of cyclohexane on titanium dioxide: an investigation of competitive adsorption and its effects on product formation and selectivity. *Appl. Catal., A* **2001**, *214* (2), 259−271. (c) Murcia-López, S.; Villa, K.; Andreu, T.; Morante, J. R. Partial Oxidation of Methane to Methanol Using Bismuth-Based Photocatalysts. *ACS Catal.* **2014**, *4* (9), 3013−3019.

(7) (a) Baek, J.; Rungtaweevoranit, B.; Pei, X.; Park, M.; Fakra, S. C.; Liu, Y.-S.; Matheu, R.; Alshmimri, S. A.; Alshehri, S.; Trickett, C. A.; Somorjai, G. A.; Yaghi, O. M. Bioinspired Metal−Organic Framework Catalysts for Selective Methane Oxidation to Methanol. *J. Am. Chem. Soc.* **2018**, *140* (51), 18208−18216. (b) Chen, X.; Li, Y.; Pan, X.; Cortie, D.; Huang, X.; Yi, Z. Photocatalytic oxidation of methane over silver decorated zinc oxide nanocatalysts. *Nat. Commun.* **2016**, *7* (1), 12273.

(8) (a) Larpent, C.; Patin, H. Oxidation of alkanes with hydrogen peroxide catalysed by iron salts or iron oxide colloids in reverse microemulsions. *J. Mol. Catal.* **1992**, *72* (3), 315−329. (b) Kang, J.; Park, E. D. Aqueous-Phase Selective Oxidation of Methane with Oxygen over Iron Salts and Pd/C in the Presence of Hydrogen. *ChemCatChem* **2019**, *11* (17), 4247−4251. (c) Szécsényi, Á.; Li, G.; Gascon, J.; Pidko, E. A. Unraveling reaction networks behind the catalytic oxidation of methane with H_2O_2 over a mixed-metal MIL-53(Al,Fe) MOF catalyst. *Chem. Sci.* **2018**, *9* (33), 6765−6773. (d) Shul'pin, G. B.; Nizova, G. V.; Kozlov, Y. N.; Gonzalez Cuervo, L.; Süss-Fink, G. Hydrogen Peroxide Oxygenation of Alkanes Including Methane and Ethane Catalyzed by Iron Complexes in Acetonitrile. *Adv. Synth. Catal.* **2004**, *346* (2−3), 317−332. (e) Ravi, M.; van Bokhoven, J. A. Homogeneous Copper-Catalyzed Conversion of Methane to Methyl Trifluoroacetate in High Yield at Low Pressure. *ChemCatChem* **2018**, *10* (11), 2383−2386. (f) Perry, S. C.; Pangotra, D.; Vieira, L.; Csepei, L.-I.; Sieber, V.; Wang, L.; Ponce de León, C.; Walsh, F. C. Electrochemical synthesis of hydrogen peroxide from water and oxygen. Nature Reviews. *Chemistry* **2019**, *3* (7), 442−458.

(9) Periana, R. A.; Taube, D. J.; Gamble, S.; Taube, H.; Satoh, T.; Fujii, H. Platinum Catalysts for the High-Yield Oxidation of Methane to a Methanol Derivative. *Science* **1998**, *280* (5363), 560−564.

(10) (a) Jones, C.; Taube, D.; Ziatdinov, V. R.; Periana, R. A.; Nielsen, R. J.; Oxgaard, J.; Goddard, W. A., III Selective Oxidation of Methane to Methanol Catalyzed, with C-H Activation, by Homogeneous, Cationic Gold. *Angew. Chem., Int. Ed.* **2004**, *43* (35), 4626−4629. (b) Periana, R. A.; Taube, D. J.; Evitt, E. R.; Löffler, D. G.; Wentrcek, P. R.; Voss, G.; Masuda, T. A Mercury-Catalyzed, High-Yield System for the Oxidation of Methane to Methanol. *Science* **1993**, *259* (5093), 340−343. (c) Basickes, N.; Hogan, T. E.; Sen, A. Radical-Initiated Functionalization of Methane and Ethane in Fuming Sulfuric Acid. *J. Am. Chem. Soc.* **1996**, *118* (51), 13111−13112.

(11) (a) Terrett, J. A.; Cuthbertson, J. D.; Shurtleff, V. W.; MacMillan, D. W. C. Switching on elusive organometallic mechanisms with photoredox catalysis. *Nature* **2015**, *524* (7565), 330−334. (b) Yamaguchi, E.; Maejima, S.; Itoh, A., Photo-Driven Catalytic Cross-Dehydrogenative Coupling (CDC)-Type Reactions. In *Heterocycles via Cross Dehydrogenative Coupling: Synthesis and Functionalization*; Srivastava, A., Jana, C. K., Eds.; Springer Singapore: Singapore, 2019; pp 413−444. (c) Sun, Z.; Tang, B.; Liu, K. K. C.; Zhu, H. Y. Direct photochemical cross-coupling between aliphatic acids and BF3K salts. *Chem. Commun.* **2020**, *56* (8), 1294−1297. (d) Qu, C.-H.; Song, G.-T.; Xu, J.; Yan, W.; Zhou, C.-H.; Li, H.-Y.; Chen, Z.-Z.; Xu, Z.-G. Merging Visible Light with Cross-Coupling: The Photochemical Direct C−H Difluoroalkylation of Imidazopyridines. *Org. Lett.* **2019**, *21* (20), 8169−8173.

(12) Hu, A.; Guo, J.-J.; Pan, H.; Zuo, Z. Selective functionalization of methane, ethane, and higher alkanes by cerium photocatalysis. *Science* **2018**, *361* (6403), 668−672.

(13) Xie, J.; Jin, R.; Li, A.; Bi, Y.; Ruan, Q.; Deng, Y.; Zhang, Y.; Yao, S.; Sankar, G.; Ma, D.; Tang, J. Highly selective oxidation of methane to methanol at ambient conditions by titanium dioxide-supported iron species. *Nat. Catal.* **2018**, *1* (11), 889−896.
(14) Kunkely, H.; Vogler, A. Photooxidation of Methane to Methanol by Perrhenate in Water under Ambient Conditions. *Z. Naturforsch. B* **2013**, *68*, 891−894.
(15) (a) Liebov, N. S.; Goldberg, J. M.; Boaz, N. C.; Coutard, N.; Kalman, S. E.; Zhuang, T.; Groves, J. T.; Gunnoe, T. B. Selective Photo-Oxygenation of Light Alkanes Using Iodine Oxides and Chloride. *ChemCatChem* **2019**, *11* (20), 5045−5054. (b) Schwartz, N. A.; Boaz, N. C.; Kalman, S. E.; Zhuang, T.; Goldberg, J. M.; Fu, R.; Nielsen, R. J.; Goddard, W. A.; Groves, J. T.; Gunnoe, T. B. Mechanism of Hydrocarbon Functionalization by an Iodate/Chloride System: The Role of Ester Protection. *ACS Catal.* **2018**, *8* (4), 3138−3149. (c) Kalman, S. E.; Munz, D.; Fortman, G. C.; Boaz, N. C.; Groves, J. T.; Gunnoe, T. B. Partial oxidation of light alkanes by periodate and chloride salts. *Dalton Trans.* **2015**, *44* (12), 5294−5298. (d) Fortman, G. C.; Boaz, N. C.; Munz, D.; Konnick, M. M.; Periana, R. A.; Groves, J. T.; Gunnoe, T. B. Selective Monooxidation of Light Alkanes Using Chloride and Iodate. *J. Am. Chem. Soc.* **2014**, *136* (23), 8393−8401. (e) Hirscher, N. A.; Ohri, N.; Yang, Q.; Zhou, J.; Anna, J. M.; Schelter, E. J.; Goldberg, K. I. *J. Am. Chem. Soc.* **2021**, *143*, 19262−19267.
(16) (a) Kim, A.-R.; Ahn, S.; Yoon, T.-U.; Notestein, J. M.; Farha, O. K.; Bae, Y.-S. Fast Cyclohexane Oxidation Under Mild Reaction Conditions Through a Controlled Creation of Redox-Active Fe(II/III) Sites in a Metal−Organic Framework. *ChemCatChem* **2019**, *11* (22), 5650−5656. (b) Fahy, K. M.; Liu, A. C.; Barnard, K. R.; Bright, V. R.; Enright, R. J.; Hoggard, P. E. Photooxidation of Cyclohexane by Visible and Near-UV Light Catalyzed by Tetraethylammonium Tetrachloroferrate. *Catalysts* **2018**, *8* (9), 403. (c) Barnard, K. R.; Bright, V. R.; Enright, R. J.; Fahy, K. M.; Liu, A. C.; Hoggard, P. E. Heterogeneous Catalysis by Tetraethylammonium Tetrachloroferrate of the Photooxidation of Toluene by Visible and Near-UV Light. *Catalysts* **2018**, *8* (2), 79.
(17) Iranpoor, N.; Adibi, H. Iron(III) trifluoroacetate as an efficient catalyst for solvolytic and nonsolvolytic nucleophilic ring opening of epoxides. *Bull. Chem. Soc. Jpn.* **2000**, *73* (3), 675−680.
(18) Guntlin, C. P.; Zund, T.; Kravchyk, K. V.; Worle, M.; Bodnarchuk, M. I.; Kovalenko, M. V. Nanocrystalline FeF3 and MF2 (M = Fe, Co, and Mn) from metal trifluoroacetates and their Li(Na)-ion storage properties. *J. Mater. Chem. A* **2017**, *5* (16), 7383−7393.
(19) Guntlin, C. P.; Ochsenbein, S. T.; Wörle, M.; Erni, R.; Kravchyk, K. V.; Kovalenko, M. V. Popcorn-Shaped FexO (Wüstite) Nanoparticles from a Single-Source Precursor: Colloidal Synthesis and Magnetic Properties. *Chem. Mater.* **2018**, *30* (4), 1249−1256.
(20) Frankiss, S. G. Nuclear Magnetic Resonance Spectra of Some Substituted Methanes. *J. Phys. Chem.* **1963**, *67* (4), 752−755.
(21) Blake, P. G.; Pritchard, H. The thermal decomposition of trifluoroacetic acid. *J. Chem. Soc. B* **1967**, No. 0, 282−286.
(22) Lambert, J. B.; Wang, G. T.; Finzel, R. B.; Teramura, D. H. Stabilization of Positive Charge by Beta-Silicon. *J. Am. Chem. Soc.* **1987**, *109* (25), 7838−7845.

https://doi.org/10.1021/acs.inorgchem.1c03086
Inorg. Chem. 2022, 61, 759−766